Crack Propagation and Intelligent Prediction in Asphalt Pavements Under Moving Loads

International Journal of Pavement Research and Technology
https://doi.org/10.1007/s42947-026-00730-9

社團法人中華鋪面工程學會
Chinese Society of Pavement Engineering

ORIGINAL RESEARCH PAPER

Crack Propagation and Intelligent Prediction in Asphalt Pavements Under Moving Loads

Zihan Jiang[1,2] · **Chong Li**[3] · **Giuseppe Lacidogna**[2]

Received: 9 June 2025 / Revised: 2 February 2026 / Accepted: 7 February 2026

Abstract

Asphalt pavements are prone to crack initiation and propagation under the interaction of moving loads and natural environmental conditions, significantly reducing their performance and lifespan. Guided by fracture mechanics theory, this study investigates the mechanisms and key influencing factors of crack propagation in asphalt pavements subjected to moving loads through an integrated approach combining finite element simulation with back propagation (BP) neural network-based prediction. A three-dimensional pavement model containing a longitudinal crack was developed in ABAQUS to analyze the evolution of stress intensity factors K_I and K_{II} at the crack tip. The influences of vehicle speed, load level, and structural parameters, including the thickness and elastic modulus of the surface, base, and sub-base layers, were examined. The results show that low-speed driving and overloading markedly increase the peak values of K_I and K_{II}, thereby accelerating crack propagation. A decrease in the thickness of the surface layer or an increase in its elastic modulus greatly raises stress intensity factors, while the influence of base and sub-base parameters is relatively limited. A decrease in surface layer thickness or an increase in its elastic modulus significantly elevates the stress intensity factors, whereas the effects of base and sub-base parameters are relatively minor. The developed BP neural network-based prediction model achieves accurate estimation of K_I and K_{II}, with average errors below 3%, thereby offering a practical and efficient tool for rapid assessment of pavement cracking resistance. These findings furnish a theoretical foundation for the optimized design of asphalt pavements and the development of maintenance strategies, while also establishing a basis for future research on crack propagation under multi-factor coupling conditions.

Keywords Asphalt pavement · Crack propagation · Stress intensity factor · Finite element analysis · Back propagation neural network

1 Introduction

Road cracks represent a primary form of damage in asphalt pavements, whose occurrence not only compromises driving safety and comfort but may also lead to traffic accidents [1–4]. Factors such as temperature and load can induce stress concentration at the crack tips. Once the local stress exceeds the material's tensile strength, crack propagation occurs, leading to further deterioration and potential structural failure of the pavement [5–7]. Additionally, environmental conditions like moisture and rainfall infiltration can accelerate this process, exacerbating pavement damage [8–10]. Therefore, investigating the propagation behavior of pavement cracks is of critical importance.

Furthermore, ensuring the long-term serviceability of asphalt pavements through continuous monitoring and timely maintenance, despite frequent budget constraints,

✉ Giuseppe Lacidogna
giuseppe.lacidogna@polito.it

Zihan Jiang
19zhjiang@stu.edu.cn

Chong Li
Chong.Li@xjtlu.edu.cn

[1] Department of Civil Engineering and Smart Cities, Shantou University, 243 University Road, Shantou, China

[2] Department of Structural, Geotechnical and Building Engineering, Politecnico di Torino, 24, Corso Duca degli Abruzzi, 10129 Turin, Italy

[3] School of AI and Advanced Computing, Xi'an Jiaotong-Liverpool University, Suzhou 215400, China

Published online: 24 February 2026

remains a primary objective for sustainable infrastructure management. Accurate estimation of pavement service life facilitates the forecasting of remaining lifespan and aids in formulating efficient maintenance plans. Methods for estimating remaining life due to different types of distress, such as edge faulting, fatigue cracking, roughness levels, pavement deflection, and layer thickness, are generally categorized as functional or structural. These methods utilize data such as the Pavement Condition Index (PCI), Pavement Surface Rating (PSR), layer thickness, and layer modulus. Various analytical approaches are available, including empirical studies, probabilistic methods, mechanistic-empirical techniques, and soft computing, all based on the pavement's history. Several studies in the literature have proposed continuous data collection methods using self-sensing sensors to enhance the accuracy of pavement condition assessments [11–14].

The formation and propagation of cracks in asphalt pavements have long been a major research focus in road engineering [15–17]. Numerous scholars have employed various methods to analyze crack propagation, including experimental methods, analytical methods, and finite element analysis [18–22]. The experimental method is widely adopted due to its effectiveness, enabling effective screening and assessment of crack behavior [23–27]. Kaplan was the first to apply fracture mechanics to the study of crack propagation in concrete [28]. With the deepening of understanding of crack propagation mechanisms, more researchers have begun to explore the influence of pavement materials on crack propagation [29]. However, experimental approaches suffer from limitations such as lengthy durations, high costs, and difficulties in conducting large-scale studies. Analytical methods, valued for their simplicity and efficiency, have also been widely applied. Hillerborg et al. [30] combined concrete fracture mechanics with discrete models to study crack propagation. Sei Ueda et al. [31] applied integral transformation methods to calculate the stress intensity factors under interactions between different composite materials. Zhong et al. [32] derived expressions for the stress intensity factors at the crack tip, highlighting the significant impact of the pavement's elastic modulus on crack propagation by integrating fracture mechanics theory, Fourier transformations, and the residue theorem. Huang et al. [33] improved the methods for three-dimensional crack mesh division and stress intensity factor calculations. Finite element analysis, as a numerical approximation tool for simplifying complex problems, has been extensively used in the study of pavements [34–36]. Yamada et al. [37] used finite element analysis to investigate the singularity at the crack tip, with the aim of revealing crack propagation patterns. Aliabadi et al. [38] modelled and analyzed the nonlinear issues of concrete cracks using boundary element methods. Chen et al. [39] studied the propagation and settlement problems of three-dimensional pavement cracks under impact loads using ABAQUS software. However, due to the complexity of crack behavior, existing studies present certain limitations. For instance, the analytical methods based on elastic layered system theory have not sufficiently accounted for stress concentration effects in crack propagation assessment. Moreover, factors such as vehicle load, speed, and temperature variations have not been accurately modeled, which affects the reliability of crack propagation predictions.

To address the limitations of the aforementioned research, this paper employs fracture mechanics theory and introduces stress intensity factors to analyze the stress field at the crack tip. A three-dimensional asphalt pavement model with longitudinal cracks was developed using the finite element software ABAQUS to determine the stress intensity factors at the crack tip and to examine the influence of pavement structure on crack propagation.

Moreover, in modern research on materials and their physic-mechanical properties, machine learning methods are increasingly being successfully applied, as evidenced in the literature. Methods like bagging and random forests leverage multiple models to enhance robustness and accuracy through algorithm aggregation. This approach has been used, for instance, in predicting the compressive strength of high-performance concrete [40]. In contrast, the back-propagation (BP) algorithm operates by minimizing prediction errors. This is achieved by adjusting the weights of the connections between neurons in a multi-layered neural network. Specifically, the BP algorithm computes the gradient of the loss function with respect to each weight via the chain rule, enabling the model to learn from prediction errors.

In recent years, machine learning (ML) techniques have been increasingly applied to predict pavement performance and damage propagation. For instance, Damirchilo et al. [41] predicted the International Roughness Index (IRI) using XGBoost on LTPP data, showing its superiority over SVR and Random Forest; Yao et al. [42] developed a reliable and interpretable ML framework for pavement prediction by integrating BorutaShap, Bayesian Neural Networks, and SHAP. Meanwhile, Mansour et al. [43] created an ensemble model for long-term Pavement Condition Index (PCI) prediction, while Zhao et al. [44] identified Gradient Boosting and ensemble methods as optimal for analyzing pavement distress and overlay strategies.

However, most existing ML-based studies focus on crack detection or material property prediction, with limited application to the direct prediction of fracture mechanics parameters such as stress intensity factors (SIFs) under moving loads. The present study differs by combining finite element simulation with a BP neural network to predict SIFs (K_I and

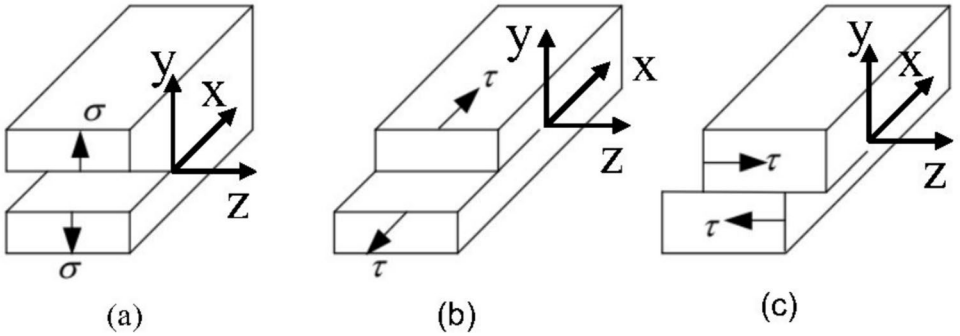

Fig. 1 Schematic diagram of three basic crack fracture modes: (**a**) Mode I, (**b**) Mode II, (**c**) Mode III

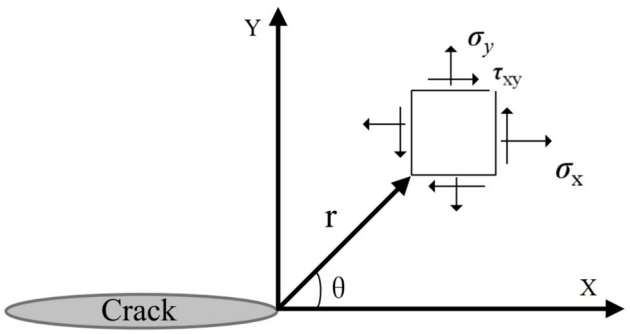

Fig. 2 Stress distribution at the crack tip

K_{II}) considering both structural and load parameters. This approach enables rapid assessment of crack propagation risk without repeated finite element analysis, offering a practical tool for pavement design and maintenance planning.

Therefore, in this paper, a BP neural network was employed to explore the effects of varying thicknesses and elastic moduli of the surface layer, base layer, and sub-base layer on crack propagation, as well as to model and predict the stress intensity factors obtained at the crack tip. Through this research, the paper aims to provide significant reference value for pavement design and maintenance.

It is acknowledged that environmental factors such as temperature cycles and moisture ingress significantly influence crack propagation. However, to establish a clear understanding of the mechanical drivers, the present study deliberately focuses on the response induced by moving loads, isolating these effects from environmental complexities. Future work will incorporate thermo-mechanical coupling to explore crack behavior under combined thermal and mechanical loading. Asphalt concrete exhibits significant viscoelastic behavior, with properties dependent on temperature and loading rate. However, this study models the asphalt layer as a linear elastic material to simplify the complex interactions of moving loads and crack propagation. This assumption isolates the geometric and dynamic effects of the load on SIFs, providing valuable qualitative insights, though it does not capture the material's rate-dependent stiffness changes. Incorporating viscoelasticity remains a key objective for future model refinement.

2 Theory of Fracture Mechanics

Fracture mechanics is a branch of solid mechanics that focuses on the strength and propagation behavior of materials containing cracks. This discipline traces its origins to the 1920s, when Griffith's work on brittle fracture in glass laid the foundational concepts, evolving into a systematic theoretical framework by the 1950s. The three fundamental parameters in this field include the stress intensity factor (SIF, K), path-independent integral (J-integral, J), and strain energy release rate (SERR, G). The stress intensity factor describes the stress state at the tip of an elastic crack, effectively eliminating the stress singularity induced by the crack. The J-integral quantifies the energy absorbed due to crack presence, while the strain energy release rate represents the energy required for the formation of new crack surfaces.

Based on the stress and displacement characteristics of cracks, they can be classified into three basic types: opening mode (Mode I), sliding mode (Mode II), and tearing mode (Mode III), as illustrated in Fig. 1. Among these, Mode I cracks are the most prevalent and critical form and have been studied most extensively. In practical engineering, many cracks do not occur as a single type but rather form as a combination of two or three types, known as compound cracks.

2.1 Stress Intensity Factor

In 1957, Irwin first introduced the concept of the Stress Intensity Factor (SIF) [45], defining it as a physical quantity that reflects the intensity of the elastic stress field at the crack tip. It depends on the crack size, the geometric features of the component, and the applied load.

Figure 2 illustrates a two-dimensional crack problem, with the crack tip located at the origin. Both a rectangular coordinate system and a polar coordinate system are established to describe the stress and displacement fields near the crack tip.

Stress field and displacement field at the tip of mode I crack:

$$\begin{cases} \sigma_x = \dfrac{K_I}{\sqrt{2\pi r}} cos\dfrac{\theta}{2}\left(1 - sin\dfrac{\theta}{2}sin\dfrac{3\theta}{2}\right) \\ \sigma_y = \dfrac{K_I}{\sqrt{2\pi r}} cos\dfrac{\theta}{2}\left(1 + sin\dfrac{\theta}{2}sin\dfrac{3\theta}{2}\right) \\ \tau_{xy} = \dfrac{K_I}{\sqrt{2\pi r}} sin\dfrac{\theta}{2}cos\dfrac{\theta}{2}cos\dfrac{3\theta}{2} \\ \tau_{xz} = \tau_{yz} = 0 \\ u = \dfrac{K_I}{2G}\sqrt{\dfrac{r}{2\pi}} cos\dfrac{\theta}{2}\left(\kappa - 1 + 2\sin^2\dfrac{\theta}{2}\right) \\ \nu = \dfrac{K_I}{2G}\sqrt{\dfrac{r}{2\pi}} sin\dfrac{\theta}{2}\left(\kappa - 1 + 2\cos^2\dfrac{\theta}{2}\right) \end{cases} \tag{1}$$

In this equation, K_I represents the stress intensity factor for Mode I cracks, while u and v denote the displacement components in the x and y directions, respectively. G represents the shear modulus of the material, while κ is a Kolosov constant defined in terms of Poisson's ratio (μ), as given by:

$$\kappa = \begin{cases} 3 - 4\mu, & \text{Plane strain} \\ \frac{3-\mu}{1+\mu}, & \text{Plane stress} \end{cases} \tag{2}$$

Stress field and displacement field at the tip of mode II crack:

$$\begin{cases} \sigma_x = -\dfrac{K_{II}}{\sqrt{2\pi r}} sin\dfrac{\theta}{2}\left(2 + cos\dfrac{\theta}{2}cos\dfrac{3\theta}{2}\right) \\ \sigma_y = \dfrac{K_{II}}{\sqrt{2\pi r}} sin\dfrac{\theta}{2}cos\dfrac{\theta}{2}cos\dfrac{3\theta}{2} \\ \tau_{xy} = \dfrac{K_{II}}{\sqrt{2\pi r}} cos\dfrac{\theta}{2}\left(1 - sin\dfrac{\theta}{2}sin\dfrac{3\theta}{2}\right) \\ \tau_{xz} = \tau_{yz} = 0 \\ u = \dfrac{K_{II}}{2G}\sqrt{\dfrac{r}{2\pi}} sin\dfrac{\theta}{2}\left(\kappa + 1 + 2\cos^2\dfrac{\theta}{2}\right) \\ \nu = \dfrac{K_{II}}{2G}\sqrt{\dfrac{r}{2\pi}} cos\dfrac{\theta}{2}\left(\kappa - 1 - 2\sin^2\dfrac{\theta}{2}\right) \end{cases} \tag{3}$$

where K_{II} represents the stress intensity factor for Mode II cracks.

For Mode I cracks, the condition for no crack propagation is as follows:

$$K_I \leq K_{IC} \tag{4}$$

where K_{IC} represents the material's fracture toughness, and the same criterion applies to Mode II cracks.

For cracks under combined Mode I and II loading, the propagation direction often deviates from the original crack plane. Pook [46] suggested that the crack tends to branch in a direction where the local Mode I stress intensity factor (K_I) is maximized, and the local Mode II component (K_{II}) is minimized. Based on the extended branch method, the equivalent Mode I stress intensity factor for a branched crack can be expressed as:

$$K_I^* = \cos\frac{\theta}{2}\left(K_I\cos^2\frac{\theta}{2} - \frac{3}{2}K_{II}\sin\theta\right) \tag{5}$$

where θ is the branch angle that satisfies $K_{II}=0$. This value K_I^* can be regarded as an equivalent SIF governing mixed-mode crack growth.

In this study, the stress intensity factors K_I and K_{II} obtained from the finite element model are used to assess crack propagation risk based on the criterion $K_I \leq K_{IC}$. This provides a theoretical basis for the following numerical simulations and neural network predictions.

3 Numerical Simulation of Asphalt Pavements

3.1 Finite Element Model by ABAQUS

ABAQUS is an internationally recognized advanced finite element analysis software, capable of handling both relatively simple linear analyses and highly complex nonlinear problems. The software provides a variety of element libraries and a wide range of material models, including metals, reinforced concrete, rock, and composites. By defining the geometric dimensions and material properties of the structure, applying loads, and setting boundary conditions, the user-defined model can be meshed, after which finite element analysis and calculations are performed.

ABAQUS primarily consists of a pre-processing and post-processing module, ABAQUS/CAE, and two simulation solvers, ABAQUS/Standard and ABAQUS/Explicit. ABAQUS/CAE provides an interactive graphical environment and includes nine modules: Part, Property, Assembly, Step, Interaction, Mesh, Load, Job, and Visualization. The first seven modules are used for pre-processing, while the Job module handles model analysis and computation. The Visualization module is dedicated to post-processing, displaying the analysis and calculation results. ABAQUS/Standard is a general-purpose analysis module widely used for solving linear and nonlinear problems, while ABAQUS/Explicit is specifically designed for dynamic simulations.

3.2 Model Dimensions and Structural Parameters

As shown in Fig. 3, a pavement finite element model with longitudinal cracks was established, with dimensions of 6 m × 6 m × 3.8 m. As shown in Table 1, the pavement is divided into four layers: a 25 cm thick asphalt pavement

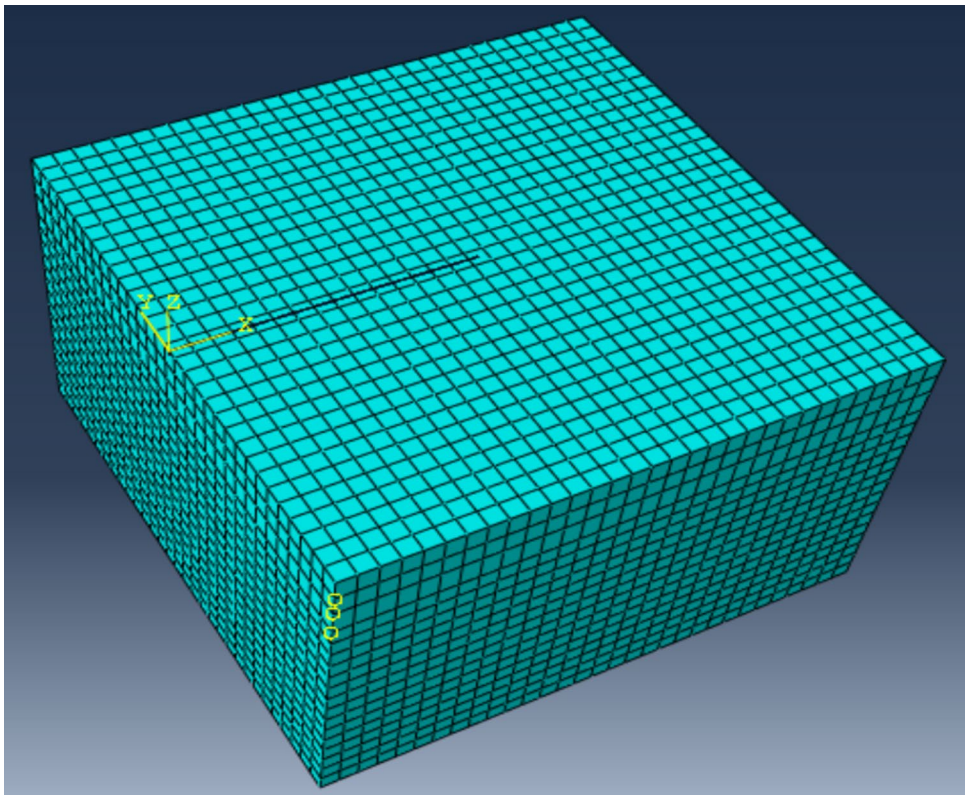

Fig. 3 Pavement model and meshing

Table 1 Pavement material parameters

Material type	Thickness (m)	Elastic modulus (MPa)	Poisson's ratio	Density (kg/m^3)
Asphalt pavement surface layer	0.25	3000	0.2	2500
Cement-stabilized crushed stone base layer	0.25	1200	0.3	2500
Cement-stabilized crushed stone sub-base layer	0.3	1000	0.35	2500
Soil subgrade	3	300	0.35	1800

surface layer, a 25 cm thick cement-stabilized crushed stone base layer, a 30 cm thick cement-stabilized crushed stone sub-base layer, and a 3 m thick soil subgrade. The moving load is applied as a pressure distribution via a user-defined DLOAD subroutine, simulating the passage of a dual-wheel assembly along the pavement centerline. Since the interaction between the two groups of wheels in a single-axle dual-wheel assembly is minimal, we only analyzed the dual wheels on one side. In the finite element analysis, this model employs C3D8R, which is a three-dimensional eight-node linear reduced integration hexahedral element. The bottom surface of the subgrade is assigned fixed boundary conditions. To mitigate boundary effects and approximate a semi-infinite domain, the side surfaces are constrained only in their normal directions. A uniform mesh of C3D8R elements was employed throughout the model. A mesh sensitivity analysis comparing element sizes of 20 cm, 15 cm, and 10 cm showed that reducing the size from 20 to 15 cm increased the peak K_I value by 5.1%, while further refinement to 10 cm resulted in only a 0.5% change. This indicates result convergence at the 15 cm size, which was therefore adopted to balance accuracy and computational efficiency.

3.3 Moving Loads

According to the JTD D50-2017 (Specifications for Design of Highway Asphalt Pavement), this study adopts the standard single axle dual-wheel assembly, specifically the BZZ-100, with a standard axle load of 100 kN and a tyre pressure of 0.7 MPa. A rectangular load is used to approximate the tyre contact area for simplified finite element modelling, with a length and width of 17.06 cm and 15.67 cm, respectively, and a spacing of 16.28 cm between the two wheels. The load equivalence diagram is shown in Fig. 4. In this study, the contact pressure of the tyres is set at 0.7 MPa, and the load is applied as a surface pressure using the DLOAD subroutine on the three-dimensional asphalt pavement model.

The moving load is applied along the longitudinal direction of the pavement, traversing directly above the pre-existing crack. The load moves at a constant speed along

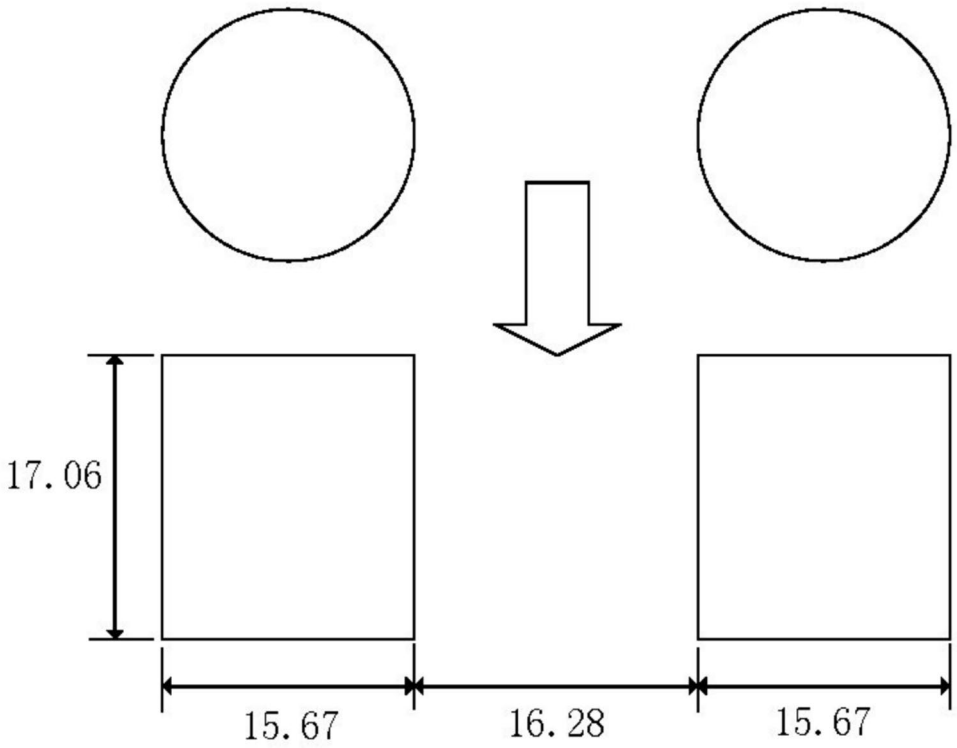

Fig. 4 Equivalent load diagram (units: cm)

a straight path parallel to the crack, with the center of the dual-wheel assembly aligned with the crack centerline.

3.4 Crack Position

Based on fracture mechanics research, this study utilizes the Extended Finite Element Method (XFEM) module in ABAQUS to enable arbitrary crack propagation without the need for the mesh to conform to the crack geometry. The initial crack configuration for the simulation was clearly defined as follows (as illustrated in Fig. 3). A pre-defined through-length longitudinal crack, with a length of 3 m and a depth of 4 cm, was embedded in the pavement model. This crack penetrates vertically through the entire thickness of the asphalt surface layer and is positioned at the center of the model in both the longitudinal and transverse directions, with its tip located precisely at the interface between the surface layer and the base layer.

The primary advantage of using XFEM in this context is that it eliminates the requirement for defining the precise path of crack propagation or refining the mesh around the crack tip, which is often necessary in traditional finite element analysis. Traditional methods typically require re-meshing or the use of singular elements to capture the stress singularity at the crack tip, leading to computational inefficiency and complexity in modeling growing cracks. In contrast, XFEM incorporates discontinuous enrichment functions (jump functions for the crack face and asymptotic functions for the crack tip) into the standard finite element approximation. This approach allows the crack to be modeled independently of the mesh, enabling it to propagate along an arbitrary, solution-dependent path during the analysis without the need for pre-defined growth planes.

In this study, the initial crack, with the dimensions and location specified above, was defined as an enriched feature within the XFEM framework. During the loading step, the model can simulate crack initiation and propagation from this pre-defined flaw based on the calculated stress fields, thereby more accurately representing the actual crack behavior in asphalt pavements.

4 Calculation and Analysis of Stress Intensity Factors

The Stress Intensity Factor (SIF) is a physical quantity that reflects the intensity of the elastic stress field at the crack tip. For Mode I cracks, when $K_I > 0$, it indicates that the crack tip is subjected to tensile forces, leading to a tendency for crack propagation; conversely, when $K_I < 0$, it suggests that compressive forces are acting on the crack tip, indicating no tendency for crack propagation. For Mode II cracks, whether $K_{II} > 0$ or $K_{II} < 0$, shear stresses may still cause further crack propagation.

4.1 Impact of Vehicle Speed on Crack Propagation

In this section, we investigate the effects of different driving speeds on crack propagation. Vehicle speeds were set at 120 km/h, 90 km/h, and 60 km/h, and the variations of K_I and K_{II} under these speeds were analyzed.

Figures 5a, b display the variation curves of stress intensity K_I and K_{II} at different speeds with the same load. As time increases and the moving load gradually approaches the crack tip, K_I increases to a peak value; as the load moves away, K_I gradually decreases. Therefore, under the action of the moving load, it is easy to induce the propagation of Mode I cracks at the tip of the longitudinal crack. Meanwhile, as the moving load reaches the tip of the crack, the stress intensity K_{II} gradually increases, and when the moving load departs from the crack tip, the absolute value of K_{II} gradually decreases. The magnitude of K_{II}, regardless of its sign, influences crack propagation, potentially promoting Mode II crack growth.

It is also noteworthy that although the duration of the moving load's effect on the crack differs at different speeds, the resulting peak values of stress intensity are generally similar. Slower moving loads result in longer load durations, which are more likely to lead to crack propagation.

This phenomenon is rooted in the viscoelastic nature of asphalt concrete and its rate-dependent mechanical response. Under a slow-moving load, the duration of stress application at the crack tip is prolonged. This allows sufficient time for viscous flow and creep deformation to occur within the asphalt material, leading to a greater accumulation of strain energy at the crack tip. According to the fundamental principle of fracture mechanics, crack propagation is driven by the energy release rate. A slower load rate thus provides a higher energy input, increasing the crack driving force. Furthermore, the extended loading time enables a more developed plastic zone at the crack tip, which can reduce the effective fracture toughness of the material. In contrast, a high-speed load is akin to an impact, where the material responds predominantly in an elastic manner; the energy is applied too rapidly for significant viscous dissipation and damage accumulation at the crack tip, resulting in a lower propensity for crack propagation despite similar peak SIF values.

The preceding analysis, based on a linear elastic material model, elucidates that vehicle speed influences the SIFs primarily through the duration of load application at the crack tip. It should be emphasized that in reality, the viscoelastic nature of asphalt concrete would introduce an additional effect: the effective modulus of the asphalt layer would increase with higher loading rates (vehicle speeds). This rate-dependency could potentially counteract or amplify the duration effects observed in our current model. Therefore, the results presented represent a fundamental scenario. A more sophisticated model incorporating viscoelastic material properties is necessary to fully quantify the synergistic

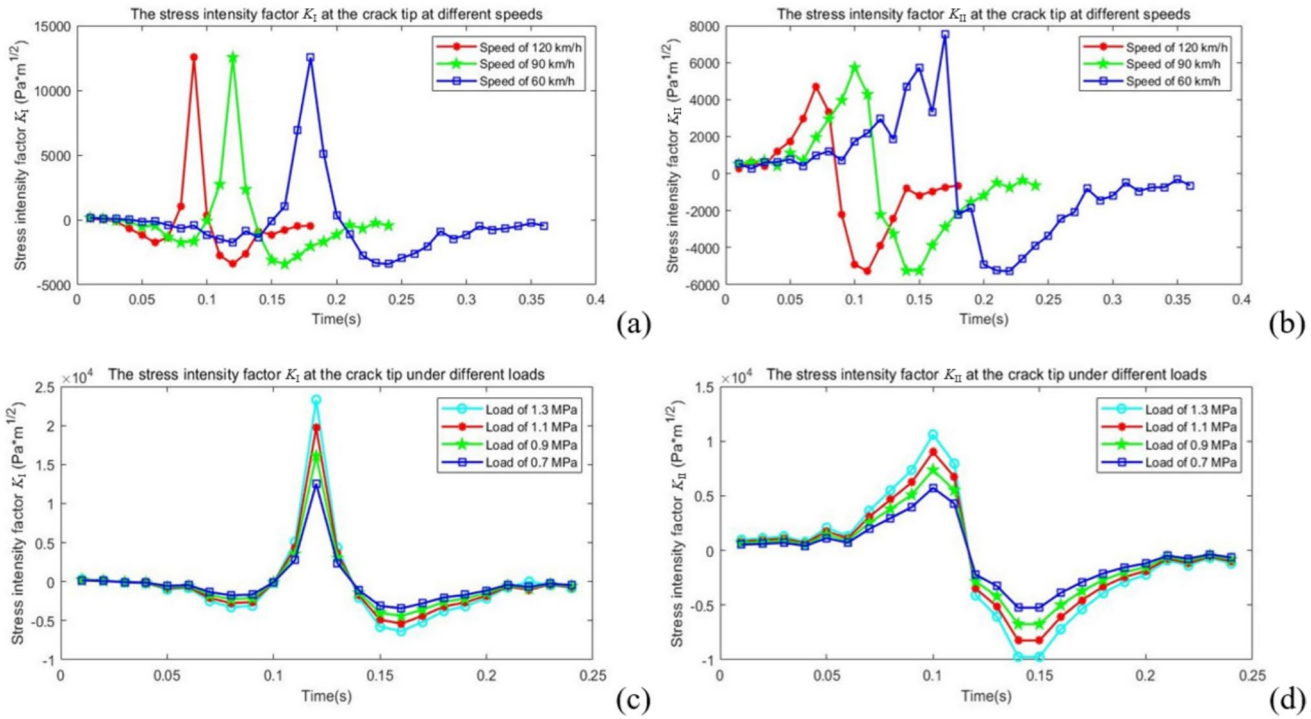

Fig. 5 Curves of stress intensity factors K_I and K_{II} under different vehicle speeds and loads: (**a**, **b**) K_I and K_{II} at different vehicle speeds, (**c**, **d**) K_I and K_{II} at different load levels

effects of loading rate and material response, which represents a promising direction for subsequent research.

4.2 Impact of Vehicle Load on Crack Propagation

As vehicles travel on the pavement, they apply various loads, including axle loads, static loads, and dynamic loads caused by vehicle vibrations. Dynamic loading in this context refers to the transient fluctuations in tire-pavement contact pressure resulting from vehicle dynamics and road surface irregularities. These fluctuations can lead to variations in the contact area and pressure magnitude, which in turn affect the stress intensity factors at the crack tip. Therefore, to study the impact of dynamic loads on pavement cracks, we can conduct simulated experiments by varying the contact pressure. Therefore, to investigate the influence of variable loading conditions, which serves as a proxy for dynamic effects, on pavement cracks, a series of simulated experiments were conducted by systematically varying the tire contact pressure.

In actual driving conditions, overloaded vehicles often increase the tyre pressure to maintain normal driving performance, resulting in higher contact pressures on the pavement. In this study, we investigate the effects of different load magnitudes on pavement crack propagation by varying contact pressures. Specifically, we use a baseline contact pressure of 0.7 MPa and examine the effects of contact pressures of 0.9 MPa, 1.1 MPa, and 1.3 MPa on crack propagation.

Figures 5c,d show the variation curves of the stress intensity factors K_{I} and K_{II} at different load magnitudes. As illustrated, with an increase in contact pressure, both K_{I} and K_{II} gradually increase. The experiments indicate that an increase in the contact pressure of moving vehicle tyres leads to higher peak values of the stress intensity factors, thereby accelerating crack propagation.

The detrimental effect of overloading can be directly explained by the fundamental definition of the stress intensity factor. The SIF (K) is proportional to the applied far-field stress (σ). An increase in tire contact pressure linearly elevates the local stress in the pavement surface layer where the crack is located. The stress fields around the crack tip (Eqs. 1 and 3) show that all stress components (σ_{x}, σ_{y}, τ_{xy}) are linearly dependent on the SIF. Therefore, overloading directly and linearly amplifies the stress concentration at the crack tip. This pushes the crack tip into a more critical stress state, significantly increasing the likelihood that the SIF will exceed the material's fracture toughness.

4.3 Impact of Surface Layer Material Parameters

In this section, we primarily investigate the influence of the surface layer parameters, including layer thickness and elastic modulus, on the propagation patterns of pavement cracks.

4.3.1 Surface Layer Thickness

As shown in Fig. 6a, when the moving load travels uniformly at the same speed, the stress intensity factor increases gradually as the load approaches the observation point over time, and decreases after the load passes. In this study, when other conditions are fixed and only the surface layer thickness is changed from 30 to 15 cm, the stress intensity factor K_{I} gradually increases with the reduction in surface layer thickness. Additionally, as illustrated in Fig. 6b, the stress intensity factor K_{II}, which reflects shear stress variation over time, initially increases to a positive peak, then quickly drops to a negative peak, and ultimately decreases gradually. As the surface layer thickness decreases, the stress intensity factor K_{II} also gradually increases.

The results indicate that the thickness of the pavement surface layer significantly influences the stress intensity factors K_{I} and K_{II}; specifically, the smaller the surface layer thickness, the larger both K_{I} and K_{II} become, making it more susceptible to crack propagation. Therefore, increasing the surface layer thickness can enhance the cracking resistance of asphalt pavements. However, in practical engineering, the cost should also be considered, and an appropriate value for the surface layer thickness should be set.

The mechanism behind the influence of surface layer thickness relates to the structural stiffness and stress distribution. A thinner surface layer has lower flexural stiffness. Under a moving load, it undergoes greater bending deformation. This bending induces higher tensile stresses at the bottom of the layer, which are directly transferred to the tip of the surface-initiated crack, significantly increasing the Mode-I SIF. Essentially, reducing the layer thickness diminishes the volume of material constraining the crack, allowing the load-induced energy to be concentrated at the crack tip. Conversely, a thicker surface layer increases the overall structural stiffness, distributing the wheel load over a wider area and effectively shielding or diluting the stress concentration at the crack tip.

4.3.2 Surface Layer Elastic Modulus

The elastic modulus is a critical performance parameter of engineering materials; from a macroscopic perspective, it quantifies a material's resistance to elastic deformation. The elastic modulus of the surface layer is one of the essential

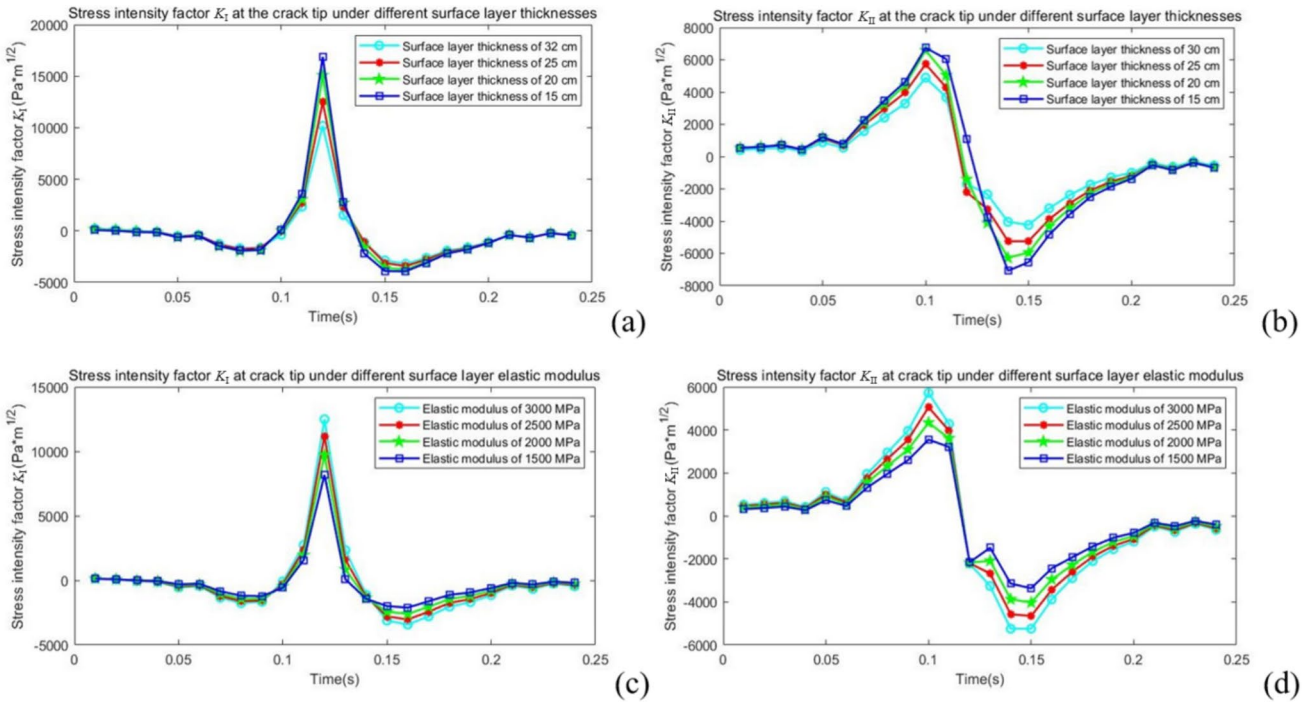

Fig. 6 Curves of stress intensity factors K_I and K_{II} at the crack tip with different surface layer thicknesses and elastic moduli: (**a**, **b**) K_I and K_{II} for different surface layer thicknesses, (**c**, **d**) K_I and K_{II} for different surface layer elastic moduli

parameters of pavement structures and significantly influences the pavement's resistance to crack deformation.

As shown in Fig. 6c, when the moving load travels at a constant speed, the stress intensity factor gradually increases as it approaches the observation point over time, and decreases as it moves away from that point. In this study, when other conditions are fixed and the elastic modulus is varied from 3000 to 1500 MPa, the stress intensity factor K_I decreases as the elastic modulus is reduced. Figure 6d also presents the variation curve of the stress intensity factor K_{II} over time. K_{II} first increases to a positive peak, then rapidly drops to a negative peak, eventually decreasing gradually. As the elastic modulus decreases, the stress intensity factor K_{II} also diminishes.

These experiments indicate that the pavement surface layer's elastic modulus significantly impacts the variations of the stress intensity factors K_I and K_{II}. The greater the elastic modulus, the larger the values of K_I and K_{II}, which increases the likelihood of crack propagation or failure. Therefore, appropriately reducing the elastic modulus of the surface layer can enhance the crack resistance of asphalt pavements.

The elastic modulus determines the stress level generated for a given strain. A higher modulus material is stiffer and will develop higher stresses under the same deformation. Since SIF is proportional to stress, a higher modulus directly results in elevated K_I and K_{II} values at the crack tip. Moreover, high-modulus materials often exhibit lower fracture toughness or, at best, a KIC that does not increase proportionally with elastic modulus. Consequently, a high-modulus surface layer leads to a higher K_I/K_{IC} ratio, increasing the risk of crack propagation. In contrast, a moderately lower modulus may accommodate greater deformation but at a lower stress level. Such materials often possess better toughness and energy-absorption capabilities, which help to inhibit crack growth.

4.4 Impact of Base Layer Material Parameters

4.4.1 Base Layer Thickness

As shown in Fig. 7a, when the moving load travels at a constant speed, the stress intensity factor gradually increases as it approaches the observation point over time and decreases as it moves away. With other conditions held constant and the base layer thickness varied from 30 to 15 cm, the stress intensity factor K_I gradually increases with the reduction in base layer thickness, although the change is relatively small. Additionally, Fig. 7b presents the variation curve of the stress intensity factor K_{II} over time; K_{II} initially increases to a positive peak, then drops rapidly to a negative peak, and finally decreases gradually. As the base layer thickness decreases, the stress intensity factor K_{II} correspondingly increases.

The experiments indicate that a smaller base layer thickness results in larger stress intensity factors K_I and K_{II},

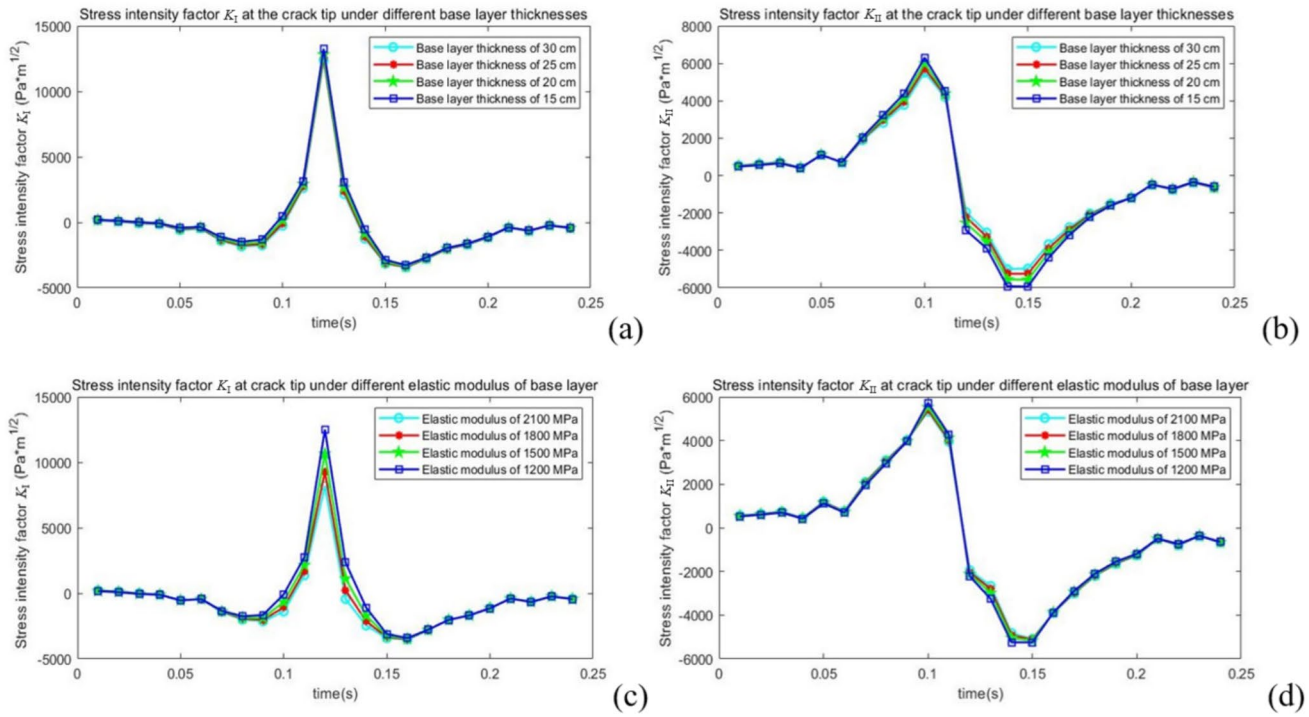

Fig. 7 Curves of stress intensity factors K_I and K_{II} at the crack tip with different base layer thicknesses and elastic moduli: (**a**, **b**) K_I and K_{II} for different base layer thicknesses, (**c**, **d**) K_I and K_{II} for different base layer elastic moduli

thereby increasing the susceptibility to crack propagation. Therefore, increasing the base layer thickness can improve the cracking resistance of asphalt pavements. However, in practical engineering, considerations of cost should also be considered, and an appropriate value for the base layer thickness should be established.

4.4.2 Base Layer Elastic Modulus

As shown in Fig. 7c, when the moving load travels at a constant speed, the stress intensity factor gradually increases as it approaches the observation point over time and decreases as it moves away. In this study, with other conditions held constant and the base layer elastic modulus varied from 2100 to 1200 MPa, the stress intensity factor K_I gradually increases as the elastic modulus decreases. Additionally, as illustrated in Fig. 7d, the stress intensity factor K_{II} first increases to a positive peak, then rapidly drops to a negative peak, and finally decreases gradually. In practice, the variation in the value of the stress intensity factor K_{II} is not particularly pronounced as the elastic modulus decreases.

Therefore, the experiments indicate that the changes in base layer thickness and elastic modulus do have an impact on the stress intensity factors K_I and K_{II} at the crack tip, although the specific effects are not very significant.

4.5 Impact of Sub-base Layer Material Parameters

4.5.1 Sub-base Layer Thickness

As shown in Figs. 8a, b, when the moving load travels at a constant speed, the stress intensity factor gradually increases as it approaches the observation point over time and decreases as it moves away. In this study, when other conditions are fixed and only the sub-base layer thickness is changed from 30 to 15 cm, the variations in stress intensity factors K_I and K_{II} are not particularly pronounced.

4.5.2 Sub-base Layer Elastic Modulus

As shown in Figs. 8c, d, when the moving load travels at a constant speed, the stress intensity factor gradually increases as it approaches the observation point over time and decreases as it moves away from that point. In this study, when other conditions are fixed and the base layer elastic modulus is varied from 1400 to 800 MPa, the changes in the stress intensity factors K_I and K_{II} are not very pronounced as the elastic modulus decreases.

The relatively minor influence of the base and sub-base layer parameters is due to their functional role and distance from the crack tip. The crack is located within the surface layer, and the SIF characterizes the local stress field at its tip. According to the principles of stress dissipation in

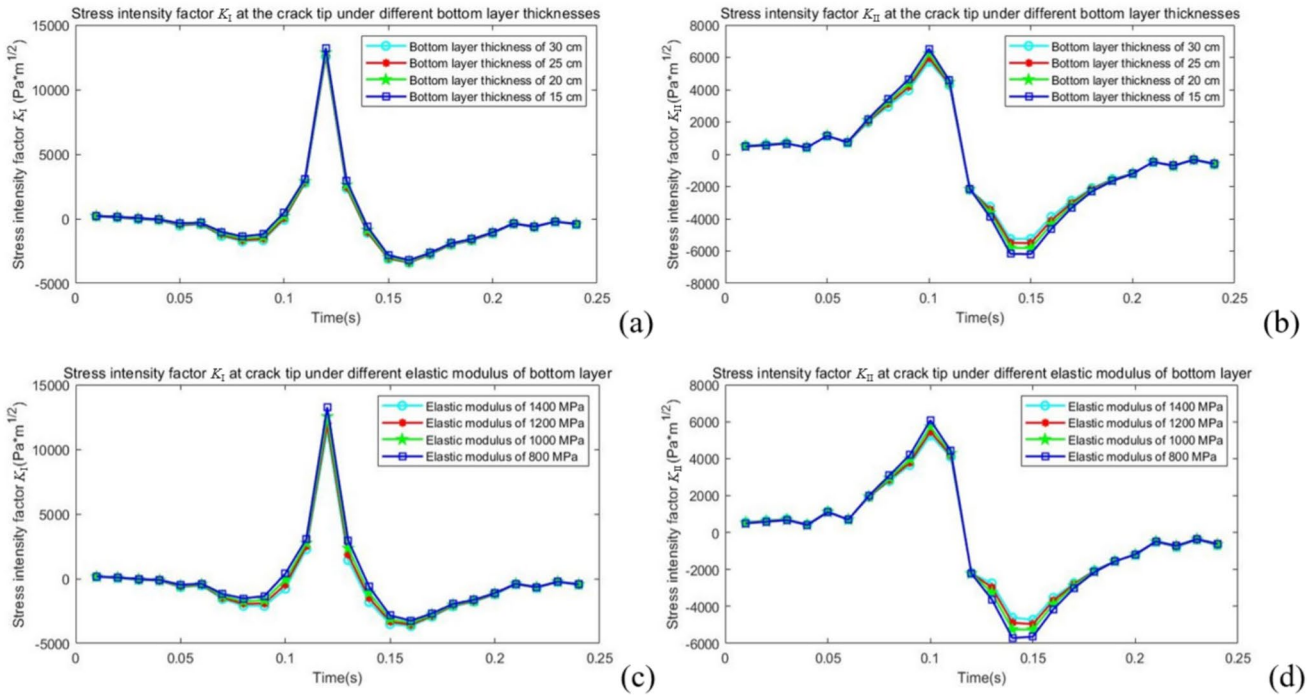

Fig. 8 Curves of stress intensity factors K_I and K_{II} at the crack tip with different sub-base layer thicknesses and elastic moduli: (**a**, **b**) K_I and K_{II} for different sub-base layer thicknesses, (**c**, **d**) K_I and K_{II} for different sub-base layer elastic moduli

layered systems, the load stress is significantly attenuated and spread out by the time it reaches the deeper layers and is then reflected back to the surface crack tip. Therefore, changes in the properties of these underlying layers have a muted effect on the intense, localized stress concentration at the crack tip. Their primary function is loading distribution and overall structural support, influencing phenomena like overall deformation and fatigue life, rather than directly controlling the stress state at a pre-existing surface crack.

5 Prediction of Stress Intensity Factors

From the previous sections, we understand that computing the stress intensity factors for the three-dimensional asphalt pavement model using ABAQUS finite element analysis is quite complex. The variations in structural parameters (such as pavement thickness and elastic modulus), speed, and load magnitudes require mesh generation for the model, making the process cumbersome. Therefore, to address this phenomenon, this study employs artificial neural networks to compute and predict stress intensity factors, thereby streamlining the calculation process.

5.1 Back Propagation (BP) Neural Network

Artificial neural networks are important models in the field of artificial intelligence, among which the Back Propagation (BP) neural network is widely used. The BP neural network has strong capabilities for processing and mapping nonlinear problems.

In this study, the selection of input parameters for the BP neural network was based on the parametric analysis presented in Sects. 4. The results indicated that the surface layer parameters (thickness and elastic modulus) have the most significant influence on the stress intensity factors, while the base layer parameters also contribute, though to a lesser extent. The influence of the sub-base layer parameters was found to be minimal. Therefore, to achieve an optimal balance between model computational efficiency and predictive accuracy, four key structural parameters were selected as model inputs: surface layer thickness, surface layer elastic modulus, base layer thickness, and base layer elastic modulus. These parameters represent the primary design variables governing pavement response in the context of this study. The output layer is focused on calculating the stress intensity factors K_I and K_{II} at the crack tip, which is why it is configured with two neurons.

The structure of the BP neural network, including the number of hidden layers and neurons, was determined through an iterative trial process aimed at optimizing performance while avoiding overfitting. A single hidden layer was found to be sufficient for capturing the nonlinear relationships in this problem. The number of neurons in the hidden layer was set to 10, which provided a good balance between model complexity and generalization capability.

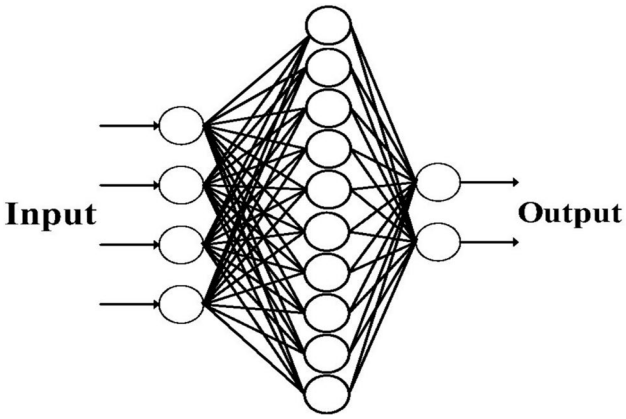

Fig. 9 Structure of BP neural network

The hyperbolic tangent sigmoid function was used as the activation function for the hidden layer, and a linear activation function was used for the output layer.

In this study, we constructed a three-layer neural network with a single hidden layer, consisting of 4 neurons in the input layer, 10 neurons in the hidden layer, and two neurons in the output layer. The structure of the BP neural network is shown in Fig. 9.

The Levenberg–Marquardt algorithm, known for its fast convergence, was selected as the training algorithm. The mean squared error was used as the performance function. We conducted experiments to calculate stress intensity factors K_I and K_{II}, resulting in a total of 256 sets of experimental data to serve as the overall sample dataset. The input parameters varied in the simulations were the surface layer thickness (15, 20, 25, 30 cm), surface layer elastic modulus (1500, 2000, 2500, 3000 MPa), base layer thickness (15, 20, 25, 30 cm), and base layer elastic modulus (1200, 1500, 1800, 2100 MPa). A full-factorial experimental design was employed, resulting in $4 \times 4 \times 4 \times 4 = 256$ unique parameter combinations. For each combination, the peak values of the stress intensity factor, K_I and K_{II}, at the crack tip under the moving load were extracted from the simulation results, forming the output data.

The dataset was normalized to the range [0, 1] to ensure stable and efficient network training. During the experiments, 20% of the data were randomly selected as the test set to evaluate the model's generalization ability. The remaining 80% were used as the training set to train and validate the proposed BP neural network. This 80–20 split is a common and effective practice in machine learning to ensure sufficient data for training while retaining a representative portion for unbiased testing.

The sample size of 256 was determined through a full-factorial design of the four key structural parameters and proved sufficient to capture the nonlinear relationship between inputs and SIFs, as demonstrated by the high prediction accuracy in Sect. 5.2. Future studies could consider expanding the dataset by incorporating additional variables or more parameter levels to further enhance model generality.

5.2 Prediction Results of Neural Network

To achieve more convenient predictions of the stress intensity factors at the crack tip, this subsection utilizes the created training and testing datasets to train and predict using the proposed BP neural network model. To comprehensively evaluate the predictive performance of the BP neural network model, in addition to the percentage error, we employed the Root Mean Square Error (RMSE) and the Coefficient of Determination (R^2) as evaluation metrics. The RMSE reflects the absolute magnitude of the prediction error, while R^2 indicates the proportion of variance in the actual data that is explained by the model.

According to Tables 2 and 3, the trained BP neural network model can effectively predict the stress intensity factors at the tips of the cracks. The maximum error for K_I is 6.88%, the minimum error is 0.31%, and the average error is approximately 2.99%. For the stress intensity factor K_{II}, the maximum error is 6.03%, the minimum error is 0.51%, and the average error is controlled at around 2.86%. Furthermore, the overall RMSE for K_I on the test

Table 2 Test results of stress intensity factor K_I at the crack tip

Surface layer thickness (cm)	Surface layer elastic modulus (MPa)	Base layer thickness (cm)	Base layer elastic modulus (MPa)	Actual K_I (MPa × $m^{1/2}$)	Predicted K_I (MPa × $m^{1/2}$)	Error (%)
25	2500	20	1200	11474	11,605	1.14
25	2000	25	1500	8336	8281	0.65
25	1500	25	2100	5666	5285	6.72
30	2500	15	1500	8339	8913	6.88
30	2000	20	2100	5486	5385	1.83
20	2500	20	1800	11384	11753	3.24
20	2000	20	1200	12116	12424	2.54
20	1500	30	1200	9406	9698	3.11
15	2500	20	1500	14592	14637	0.31
15	2000	30	2100	9682	10015	3.44

Table 3 Test results of stress intensity factor K_{II} at the crack tip

Surface layer thickness (cm)	Surface layer elastic modulus (MPa)	Base layer thickness (cm)	Base layer elastic modulus (MPa)	Actual K_{II} (MPa × $m^{1/2}$)	Predicted K_{II} (MPa × $m^{1/2}$)	Error (%)
25	2500	20	1200	5300	5232	1.28
25	2000	25	1500	4241	4020	5.20
25	1500	25	2100	3448	3240	6.03
30	2500	15	1500	4673	4821	3.17
30	2000	20	2100	3694	3712	0.51
20	2500	20	1800	5937	5837	1.67
20	2000	20	1200	5210	5075	2.57
20	1500	30	1200	3875	3717	4.05
15	2500	20	1500	6336	6422	1.37
15	2000	30	2100	4846	4983	2.82

set is 0.324 MPa·$m^{1/2}$, with an R^2 value of 0.986. For K_{II}, the RMSE is 0.298 MPa·$m^{1/2}$, with an R^2 value of 0.982. These metrics collectively confirm the high accuracy and strong explanatory power of the established BP neural network model. Therefore, the results demonstrate that the BP neural network provides a feasible, accurate, and practical approach for predicting stress intensity factors, which is a crucial step in assessing crack propagation risk in asphalt pavements (see Tables 2 and 3).

The trained BP neural network model can serve as a fast surrogate model for optimizing pavement design against cracking. By defining an objective function that minimizes the equivalent stress intensity factor K_I^*, and setting constraints based on material availability and cost, optimization algorithms can be used to identify optimal combinations of layer thickness and modulus. This approach provides a practical tool for designing crack-resistant pavement structures and will be explored in future work.

6 Discussion

6.1 Equivalent Stress Intensity Factor

Although the current study primarily analyzes the separate values of K_I and K_{II} to elucidate their individual influences on the crack tip stress field, the fracture process under moving loads is inherently a mixed-mode (I/II) problem. As established by Pook (1980), a fundamental principle in fracture mechanics is that cracks in isotropic materials tend to propagate in a direction that maximizes the local Mode I stress intensity factor of a potential branch crack, effectively transforming the mixed-mode problem into an equivalent Mode I problem. This equivalent SIF, often denoted as K_I^*, provides a unified criterion for predicting crack initiation and growth under combined loading conditions.

For the longitudinal crack investigated in this model, while the propagation path may remain self-similar, the driving force is still a combination of Modes I and II. The use of an equivalent SIF, such as the one derived from the maximum tangential stress criterion or Pook's branch crack theory, would synthesize the contributions of K_I and K_{II} into a single, more physically representative parameter. The findings of this study, which systematically quantify the effects of various factors on K_I and K_{II}, provide the essential foundational data required for calculating any such equivalent SIF in subsequent analysis. The developed BP neural network model, capable of accurately predicting both K_I and K_{II}, could be readily extended to output an equivalent K_I^*, thereby offering a more robust tool for pavement lifetime assessment against mixed-mode fracture.

Therefore, a key direction for future work will be to incorporate this unified criterion by selecting and applying an appropriate equivalent SIF formula to our dataset, re-evaluating the crack propagation risk based on this new metric, and extending the prediction model to directly forecast K_I^*. Such an advancement would be particularly valuable for predicting the branching behavior of inclined or non-planar cracks, a frequent phenomenon in actual pavement damage, thereby significantly enhancing the model's practical applicability for comprehensive pavement integrity evaluation and remaining life prediction.

6.2 Mechanistic Explanation

This study systematically reveals the key factors influencing crack propagation under moving loads through finite element simulation and provides an efficient prediction tool via a BP neural network. The deeper mechanistic analysis offered herein provides universal insights for pavement design.

Fundamentally, all influencing factors alter the balance between the crack driving force (quantified by SIF) and the material's resistance to cracking (fracture toughness, KIC). Low speed and overload primarily act by increasing the energy input and stress intensity at the crack tip, thus increasing the driving force. The surface layer parameters directly govern the structural response that determines how

much of the load stress is concentrated at the crack tip. A critical finding is the "local dominance" principle: the material and geometric properties of the layer containing the crack are paramount. This finding has direct implications for maintenance and rehabilitation strategies, suggesting that interventions should focus on the surface layer for surface-initiated cracks.

An important design implication arises from the finding that a high-modulus surface layer increases crack propagation risk. This presents a classic conflict in pavement design: high modulus is often desired for resistance to rutting, while crack resistance may benefit from a more flexible and tough material. This highlights the need for balanced or functionally graded design approaches, where the surface layer is optimized for cracking resistance, and the intermediate layers are optimized for stiffness and rutting resistance.

The successful application of the BP neural network demonstrates that despite the complexity of the fracture process, the relationship between key mechanistic parameters and the crack-tip response (SIF) is deterministic and can be captured by a data-driven model. This bridges mechanistic understanding with practical predictive tools.

It should be noted that the current BP model focuses on structural parameters as inputs, with load magnitude and vehicle speed held constant at standard design values. This approach aligns with common pavement design practice, where designers evaluate structural alternatives under specified standard loading conditions (e.g., BZZ-100 with 0.7 MPa contact pressure). While load and speed are important operational variables, their inclusion would shift the model toward a real-time assessment tool rather than a design-oriented one. Future work could extend the model to incorporate these variables, along with environmental factors such as temperature, to support more comprehensive pavement performance prediction under varying traffic and climate conditions.

7 Conclusions and Prospects

This paper utilizes fracture mechanics theory and ABAQUS finite element analysis software to develop a three-dimensional asphalt pavement model, integrating stress intensity factor analysis and BP neural network predictions to investigate crack propagation patterns and influencing factors under moving loads. Key conclusions include:

(1) Low-speed driving exacerbates crack propagation by prolonging the load duration, allowing for greater viscoelastic energy accumulation and damage at the crack tip. Overloading linearly intensifies the crack-tip stress field, rapidly elevating the stress intensity factors (K_{I} and K_{II}) and pushing the crack toward unstable growth. Both factors significantly increase the crack driving force.
(2) The reduction of surface layer thickness lowers the bending stiffness, leading to stress concentration at the crack tip. An increase in the surface layer's elastic modulus directly raises the stress level under load. These two parameters are the most sensitive because they directly control the mechanical environment at the crack tip. In contrast, changes in base and sub-base layer parameters have a limited mechanistic influence on the stress field of a surface crack due to stress dissipation and their distance from the crack.
(3) The BP neural network model effectively mapped the complex, non-linear relationships between the key design parameters and the crack-tip SIFs, confirming the feasibility of a mechanics-informed data-driven approach for rapid pavement performance assessment. The BP neural network model successfully predicts the crack tip stress intensity factors K_{I} and K_{II} with an average error of less than 3%. The findings provide theoretical insights for asphalt pavement design and maintenance, recommending a focus on optimizing surface layer structural parameters and controlling overloaded vehicles. Maintenance efforts should prioritize low-speed heavy-load sections, with prompt repairs of minor cracks to delay propagation.

A recognized limitation of this study is the exclusion of temperature variations, which are known to significantly affect asphalt material properties and crack behavior. Future research should integrate thermal effects into the finite element model to better simulate real-world conditions and provide a more comprehensive understanding of crack propagation. This study serves as a preliminary demonstration of combining finite element simulation with a BP neural network to predict crack-tip stress intensity factors. While the current model focuses on material and structural parameters, it establishes a flexible framework that can be extended in the future to include crack morphological features such as length, depth, and inclination. The neural network approach shows great promise for efficiently handling high-dimensional parameter studies, which will be essential for comprehensive fracture assessment in practical pavement engineering.

Acknowledgements The authors wish to acknowledge the International Training Program for Outstanding Young Scientific Research Talents of Shantou University, and the sponsorship guaranteed with basic research funds provided by Politecnico di Torino, Italy for their aids in this work.

Author Contributions Zihan Jiang: Writing—original draft, Validation, Methodology, Investigation, Formal analysis, Data curation.

Chong Li: Writing—review & editing, Resources, Methodology, Investigation, Funding acquisition. Giuseppe Lacidogna: Writing—review & editing, Project administration, Methodology, Conceptualization.

Funding Open access funding provided by Politecnico di Torino within the CRUI-CARE Agreement. This work was supported by the Research Development Fund of Xi'an Jiaotong-Liverpool University under Grant RDF-24-01-097.

Data Availability Available upon reasonable request from the corresponding author.

Code Availability Available upon reasonable request from the corresponding author.

Declarations

Conflict of Interest The authors have no competing interests to declare that are relevant to the content of this article.

Ethical Approval Not applicable.

Consent to Participation Not applicable.

Consent for Publication Not applicable.

References

1. Múčka, P. (2018). Sensitivity of road unevenness indicators to short wavelength distresses in Portland cement concrete surfaces. *International Journal of Pavement Engineering, 19*(10), 901–916.
2. Xing, J., Liu, Y., & Zhang, G. Z. (2024). Concrete highway crack detection based on visible light and infrared silicate spectrum image fusion. *Sensors, 24*(9), Article 2759.
3. He, X., Tang, Z., Deng, Y., et al. (2023). UAV-based road crack object-detection algorithm. *Automation in Construction, 154*, Article 105014.
4. Fan, Z., Li, C., Chen, Y., et al. (2020). Automatic crack detection on road pavements using encoder-decoder architecture. *Materials, 13*(13), Article 2960.
5. Yang, S. Y., Gao, X. G., & Zhang, L. Y. (2017). Transient analysis on reflective crack of highway semi-rigid pavement caused by temperature change. *Key Engineering Materials, 4466*, 163–168.
6. Que, Y., Dai, Y., Ji, X., et al. (2023). Automatic classification of asphalt pavement cracks using a novel integrated generative adversarial networks and improved VGG model. *Engineering Structures, 277*, Article 115406.
7. Du, J., Ali, R., Zhou, Z., et al. (2021). Enhancement effect of the aggregate particles on the low-temperature cracking resistance of the asphalt mortar. *Construction and Building Materials, 290*, Article 123225.
8. Du, J., & Fu, Z. (2024). Influence of crack configurations of asphalt mortar on the loading response characteristics of cracks under low-temperature conditions. *Engineering Fracture Mechanics, 309*, Article 110386.
9. Madeh Piryonesi, S., & El-Diraby, T. (2021). Using machine learning to examine impact of type of performance indicator on flexible pavement deterioration modeling. *Journal of Infrastructure Systems, 27*(2), Article 04021005.
10. Du, J., & Li, F. (2024). Propagation characteristics of dispersion cracks in asphalt concrete at low temperatures. *Journal of Materials in Civil Engineering, 36*(7), Article 04024179.
11. Adresi, M., Tulliani, J., Lacidogna, G., & Antonaci, P. (2021). A novel life prediction model based on monitoring electrical properties of self-sensing cement-based materials. *Applied Sciences, 11*(11), Article 5080.
12. El-Din, H., & Al-Atroush, M. (2025). A Review study of intelligent road crack detection: algorithms and systems. *International Journal of Pavement Research and Technology*. https://doi.org/10.1007/s42947-025-00556-x
13. Cafiso, S., Di Graziano, A., Fedele, R., et al. (2020). Sensor-based pavement diagnostic using acoustic signature for moduli estimation. *International Journal of Pavement Research and Technology, 13*, 573–580.
14. Roy, S. (2025). Soft computing-based optimization using ANFIS, ANN, and RSM to predict the strength of polymer adjusted thin layer asphalt for internet of road things (IoRT). *International Journal of Pavement Research and Technology*. https://doi.org/10.1007/s42947-025-00533-4
15. Gürkan, D., & Burhan, E. (2022). A new mobile convolutional neural network-based approach for pixel-wise road surface crack detection. *Measurement, 195*, Article 111119.
16. Liu, J., Zhao, Z., Lv, C., et al. (2022). An image enhancement algorithm to improve road tunnel crack transfer detection. *Construction and Building Materials, 348*, Article 128583.
17. Gao, X., & Tong, B. (2022). MRA-Unet: Balancing speed and accuracy in road crack segmentation network. *Signal, Image and Video Processing, 17*(5), 2093–2100.
18. Yan, G., Ye, Z., Wang, W., et al. (2021). Numerical analysis on distribution and response of acceleration field of pavement under moving load. *International Journal of Pavement Research and Technology, 14*, 519–529.
19. Jiang, Z., Zhu, Z., Accornero, F., et al. (2024). Multi-technique analysis of seawater impact on the performance of calcium sulphoaluminate cement mortar. *Construction and Building Materials, 443*, Article 137717.
20. Zhou, Y., Gu, Z., Li, L., et al. (2025). Intelligent asphalt pavement crack detection with 2D and 3D feature fusion using d–s evidence theory. *International Journal of Pavement Research and Technology*. https://doi.org/10.1007/s42947-025-00561-0
21. Wang, C., Jiang, Z., Accornero, F., et al. (2025). Influence of seawater and salt ions on the properties of calcium sulfoaluminate cement. *Journal of Materials in Civil Engineering, 37*(6), Article 04025156.
22. Jiang, Z., Zhu, Z., Friedrich, L. F., et al. (2026). Multi-technical analysis of damage process in GFRP-bar reinforced concrete beam. *Engineering Structures, 348*, Article 121803.
23. Wang, C., Zhou, S., Jiang, Z., et al. (2026). Multi-technology investigation on damage mechanisms in hybrid reinforced concrete beams: Synergistic effects of reinforcement and fiber content. *Construction and Building Materials, 506*, Article 144820.

24. Jiang, Z., Zhu, Z., Lacidogna, G., et al. (2025). Experimental validation and fracture mechanics analysis of an innovative UHPC-based material for structural strengthening. *Mechanics Research Communications*. https://doi.org/10.1016/j.mechrescom.2025.104603
25. Si, C., Cao, H., Fan, T., et al. (2024). Study on crack propagation behavior of bridge deck asphalt pavement. *Construction and Building Materials, 425*, Article 136136.
26. Jiang, Z., Zhu, Z., Accornero, F., et al. (2025). Acoustic emission and digital image correlation evidence of size effects on the compression failure of concrete. *Magazine of Concrete Research, 77*(17–18), 1060–1072.
27. Zhu, Z., Jiang, Z., & Accornero, F. (2025). Size-scale and time-scale effects on the failure of UHPC-strengthened reinforced concrete beams. *Structures, 78*, Article 109248.
28. Kaplan, M. (1961). Crack propagation and the fracture of concrete. *ACI Journal Proceedings*, 58–61.
29. Paris, P., & Erdogan, F. (1963). Critical analysis of crack propagation laws. *Journal of Basic Engineering, 85*(4), 528–534.
30. Hillerborg, A., Modéer, M., & Petersson, P. (1976). Analysis of crack formation and crack growth in concrete by means of fracture mechanics and finite elements. *Cement and Concrete Research, 3*, 773–778.
31. Ueda, S. (2002). The surface crack problem for a layered plate with a functionally graded nonhomogeneous interface. *Journal of Solid Mechanics and Material Engineering, 45*(3), 371–378.
32. Zhong, Y., Gao, Y., & Li, Z. (2013). Analytic solution of cement concrete pavement with crack perpendicular to the interface. *Journal of Wuhan University of Technology (Transportation Science & Engineering), 37*(6), 1158–1162.
33. Huang, R., Yang, X., Lu, B., et al. (2019). Numerical calculation method for stress intensity factor of 3-D crack front. *Ship Science and Technology, 41*(2), 9–13.
34. Pirmohammad, S., & Majd-Shokorlou, Y. (2020). Finite element analysis of road structure containing top-down crack within asphalt concrete layer. *Journal of Central South University, 27*(1), 242–255.
35. Wang, H., Wu, Y., Yang, J., et al. (2021). Numerical simulation on reflective cracking behavior of asphalt pavement. *Applied Sciences, 11*(17), 7990.
36. Gao, H., Zhang, L., Zhang, D., et al. (2021). Mechanical properties of fiber-reinforced asphalt concrete: Finite element simulation and experimental study. *E-Polymers, 21*(1), 533–548.
37. Yamada, Y., Ezawa, Y., Nishiguchi, I., et al. (1979). Reconsiderations on singularity or crack tip elements. *International Journal for Numerical Methods in Engineering, 14*(10), 1525–1544.
38. Aliabadi, M., & Saleh, A. (2002). Fracture mechanics analysis of cracking in plain and reinforced concrete using the boundary element method. *Engineering Fracture Mechanics, 69*(2), 267–280.
39. Chen, Y., Tong, C., Feng, J., et al. (2019). Dynamic analysis on cement concrete pavement with initial cracks under impact loading. *Journal of Beijing University of Aeronautics and Astronautics, 045*(007), 1474–1480.
40. Han, Q., Gui, C., Xu, J., & Lacidogna, G. (2019). A generalized method to predict the compressive strength of high-performance concrete by improved random forest algorithm. *Construction and Building Materials, 226*, 734–742.
41. Damirchilo, F., Hosseini, A., Mellat Parast, M., et al. (2021). Machine learning approach to predict international roughness index using long-term pavement performance data. *Journal of Transportation Engineering, Part B: Pavements, 147*(4), Article 04021058.
42. Yao, L., Leng, Z., Jiang, J., et al. (2022). Modelling of pavement performance evolution considering uncertainty and interpretability: A machine learning based framework. *International Journal of Pavement Engineering, 23*(14), 5211–5226.
43. Mansour, E., Dhasmana, H., Mousa, M. R., et al. (2024). Machine learning-based technology for asphalt concrete pavement performance decision-making in hot and humid climates. *Construction and Building Materials, 442*, Article 137625.
44. Zhao, J., & Wang, H. (2025). Machine learning based pavement performance prediction for data-driven decision of asphalt pavement overlay. *Structure and Infrastructure Engineering, 21*(6), 940–955.
45. Irwin, G. (1957). Analysis of stresses and strains near end of a crack traversing a plate. *Journal of Applied Mechanics, 24*, 362–364.
46. Pook, L. (1980). The significance of mode 1 branch cracks for combined mode failure. *Fracture and fatigue* (pp. 143–153). Elsevier.

Zihan Jiang is currently a PhD student at the Department of Structural, Geotechnical and Building Engineering (DISEG), Politecnico di Torino, Italy. He is also enrolled in a double-degree PhD program between Politecnico di Torino and Shantou University, China. His research interests include Nondestructive Testing, Fracture Mechanics, and Structural Health Monitoring.

Chong Li is an Assistant Professor at the School of AI and Advanced Computing, Xi'an Jiaotong-Liverpool University. He holds a PhD from Shantou University (jointly supervised at Sapienza University of Rome). His research interests include Machine Learning, Computer Vision, and Computational Civil Engineering.

Giuseppe Lacidogna is a Fellow of the European Academy of Sciences and achieved the National Academic Qualification as Full Professor of Structural Mechanics in Italy in 2018. He has been an Associate Professor in Structural Mechanics at the Department of Structural, Geotechnical and Building Engineering (DISEG), Politecnico di Torino, since 2011. He received his PhD in Structural Engineering from Politecnico di Torino in 1994. His research interests include Acoustic Emission Methods for Damage Identification, Critical Phenomena from Structural Mechanics to Geophysics, and Damage Diagnosis in Structures and Construction Materials.